EFFECT OF Nd ADDITION ON THE MICROSTRUCTURE AND CYCLIC OXIDATION BEHAVIOR OF NiAl–Cr(Mo) EUTECTIC ALLOYS

Mehmet Sahin Atas and Mehmet Yildirim
Department of Metallurgical and Materials Engineering, Faculty of Engineering and Natural Sciences, Konya Technical University, 42130 Konya, Turkey

https://doi.org/10.1007/s40962-023-01102-w

Abstract

The effect of a minor amount of rare-earth element Nd addition (0.1 at%) on the microstructural properties, microhardness, and cyclic oxidation resistance of NiAl–Cr(Mo) alloy is investigated in detail. The microstructure of investigated alloys is composed of NiAl-based dendrites and a eutectic mixture whose components are NiAl and Cr(Mo) phases. The minor amount of Nd addition refines the microstructure and increases the microhardness considerably. The results of the cyclic oxidation tests reveal that the surface scales of both alloys are mainly consisted of α-Al_2O_3 and little amount of Cr_2O_3. A Cr(Mo)-rich layer is observed in the metal/oxide interface. With Nd addition, the oxidation resistance of Ni–33Al–31Cr–3Mo alloy is strongly improved. The Nd-added alloy exhibits lower oxidation mass gain and increased scale adherence.

Keywords: *NiAl, eutectic, microstructure, cyclic oxidation*

Introduction

The B2-type ordered NiAl intermetallic compound exhibits excellent properties including high melting temperature, low density, good thermal conductivity, high Young's modulus, high corrosion, and oxidation resistance.[1–4] Therefore, NiAl is considered a potential material to replace Ni-based superalloys in aerospace turbine blade applications.[5–7] However, the brittleness and low fracture strength at room temperature and inadequate strength and creep resistance at high-temperature handicap its commercial application.[3,5,8] Alloying can be considered to be an efficient method to improve the insufficient properties.

Previous studies have presented that NiAl–Cr(Mo) eutectic alloys exhibit enhanced high-temperature strength and room-temperature fracture toughness. However, the elevated temperature strength is still insufficient for advanced aerospace turbine applications.[1–4] Thus, further alloy design and development are still needed. Previous investigations have shown that microalloying NiAl–Cr(Mo) alloys with rare earth (RE) elements (Ho, Dy, Nd, etc.,) is highly beneficial to room-temperature mechanical properties.[6,7,9–12]

On the other hand, oxidation at a high temperature can cause severe degradation and can lead to structural failure.[13–16] Although extensive studies on the oxidation behavior of NiAl have been performed, only limited information is present in the literature on the oxidation behavior of NiAl-Cr(Mo) eutectic alloys containing a minor amount of RE. To our best knowledge, Zhang et al.[7] studied the cyclic oxidation resistance of Dy-added NiAl–31Cr–3Mo alloy. They showed a two-layer oxide scale formed: a continuous Al_2O_3 surface layer and a Cr-rich layer between the metallic substrate and Al_2O_3 scale. They also showed that the oxidation resistance of Dy-added alloy is much higher than that of the based alloy. In addition, Zheng-sheng et al.[12] investigated the oxidation behavior of NiAl–Cr(Mo)–Hf–Ho alloy in the temperature range of 900–1150 °C. They showed that a continuous α-Al_2O_3 scale was formed in the temperature range of 900–1100 °C. Similar to Dy addition, Ho addition also increased the oxidation resistance.

However, no reports have studied the effect of the rare earth element Nd addition on the cyclic oxidation behavior of NiAl–Cr(Mo) eutectic alloys up to now. So the aim of

Received: 05 April 2023 / Accepted: 09 June 2023
Published online: 19 July 2023

this present study is to investigate the effect of a minor amount (0.1 at%) of Nd addition on the microstructural properties, microhardness, and cyclic oxidation behavior of Ni–33Al–31Cr–3Mo alloy. The rare-earth element concentration is an important parameter for NiAl–Cr(Mo) based alloys. For minor additions, in the vicinity of 0.1–0.2 at%, the alloy would show optimum mechanical properties with increased strength/hardness and enhanced ductility. However, if the amount of rare-earth element increases the alloy would become extremely brittle.[5] Thus, the Nd concentration is chosen as 0.1 at% in order to avoid brittleness.

Experimental Procedure

Sample Production

Ni–Al–Cr–Mo and Ni–Al–Cr–Mo–Nd alloys were produced by vacuum arc melting utilizing a tungsten electrode and a water-cooled copper tray. The nominal compositions of the studied alloys are listed in Table 1. 15 g buttons were produced utilizing high-purity starting materials: Ni (shot, 3–25 mm dia., 99.95%), Al (shot, irregular shape, 15 mm dia., 99.9%), Cr (pieces, 3–12 mm, 99.2%), Mo (wire, 2.0 mm, 99.95 %) and Nd (ingot, 99.1%).

To prevent oxidation, the high-purity Ar gas was introduced to the chamber before melting. The buttons were flipped and re-melted at least four times to ensure good chemical homogeneity. The weight losses after arc melting were less than 0.2 wt%. As a result of arc melting, a product weighing 15 g and in the form of a button was obtained. Then, the buttons were cut into slices of $10 \times 10 \times 2$ mm^3 thickness by electrical discharge machining (EDM) for heat treatment, characterization, and oxidation tests. Then, the specimens were heat-treated in laboratory air: (i) at 1250 °C for 48 h /furnace cooled (HT-I) and (ii) at 1250 °C for 48 h/water quenched and subsequently aged at 1050 °C for 24h/furnace cooled (HT-II).

Characterization

The microstructural examination of as-cast and heat-treated specimens were performed by Zeiss Evo LS-10 model scanning electron microscope (SEM) attached to an energy dispersive x-ray spectrometer (EDS). Prior to the microstructural examination, specimens were mounted in bakelite, ground to 2000 grit using SiC papers, and then polished with 1 μm Al_2O_3 suspension. Finally, specimens were etched with a %5 Nital solution. The phase analysis was conducted by X-ray diffraction (XRD) utilizing Cu-Kα radiation with a Bruker D8 model diffractometer.

The Vickers microhardness measurements were carried out with a Microbul 1000D model microhardness tester using a load of 200 g and a dwell time of 10 s. At least eight individual indentations on polished specimens were performed to obtain an average value.

Table 1. Nominal Compositions of the Alloys

Elements	Ni–Al–Cr–Mo		Ni–Al–Cr–Mo–Nd	
	(at%)	(wt%)	(at%)	(wt%)
Ni	33	41.0	33	40,9
Al	33	18.8	33	18.8
Cr	31	34.1	30.9	33.9
Mo	3	6.1	3	6.1
Nd	–	–	0.1	0.3
Total	100	100	100	100

Cyclic Oxidation Tests

For the investigation of the oxidation behavior by cyclic oxidation tests, specimens with the dimensions of $10 \times 10 \times 2$ mm^3 were used. To achieve uniform oxidation, all surfaces of the specimens were ground (up to 2000 grit), polished (1 μm Al_2O_3), ultrasonically cleaned in acetone, and dried in air. Cyclic oxidation tests were carried out at 1000 °C in a muffle furnace under laboratory air for a maximum time of 25 cycles. One cycle consists of heating the sample to 1000 °C at a heating rate of 10 °C/min, holding at 1000 °C for 1h and fast cooling (nearly 45–50 °C/min) to ambient temperature. After the tests, mass gains/losses of the specimens were recorded using an electronic balance with an accuracy of 0.01 mg. Finally, the characterization of the oxidation products was performed. A detailed description of the characterization could be found elsewhere.[17–21]

Results and Discussion

Microstructural Evolution

The microstructures of as-cast and heat-treated NiAl–Cr(Mo) and NiAl–Cr(Mo)–Nd alloys are shown in Figure 1. The microstructure of NiAl–Cr(Mo) alloy is comprised of NiAl-based equiaxed dendrites (dark phase) and cellular eutectic mixture, composed of rod-like or lamella Cr(Mo) phase (light phase) and NiAl matrix phase. In the eutectic cell, NiAl and Cr(Mo) phases form a radially emanating pattern from the cell core to the eutectic cell boundary. The NiAl and Cr(Mo) phases are much coarser at the intercellular zone compared to those in the cell interior. The eutectic cell boundaries are the last solidification areas and exhibit much coarser morphology.[22,23] In addition, fine Cr(Mo) precipitates are present within the NiAl dendrites. The chemical composition of the phases in NiAl–Cr(Mo) alloy is analyzed with EDS and shown in Figures 2, 3. The results of the EDS analysis indicate that the atomic ratio of Ni:Al is close to 1 and Mo tends to dissolve in the Cr phase.

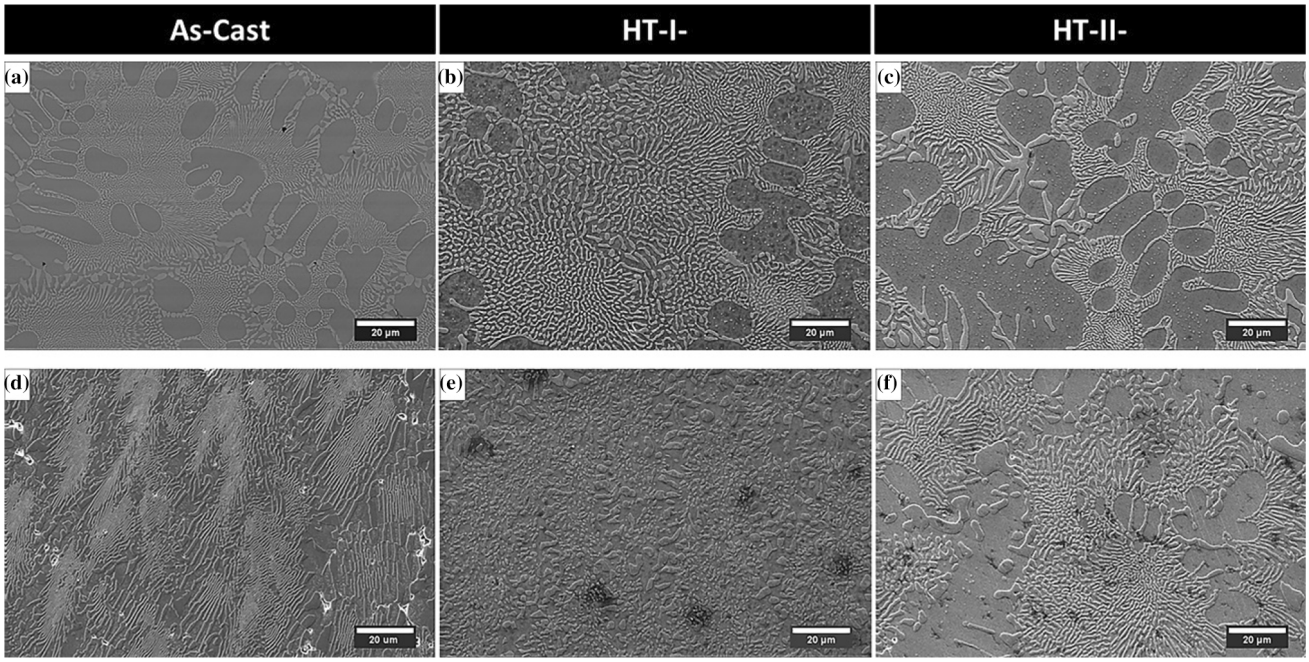

Figure 1. SEM micrographs of as-cast and heat-treated alloys: (a–c) NiAl–Cr(Mo) and (d–f) NiAl–Cr(Mo)–Nd.

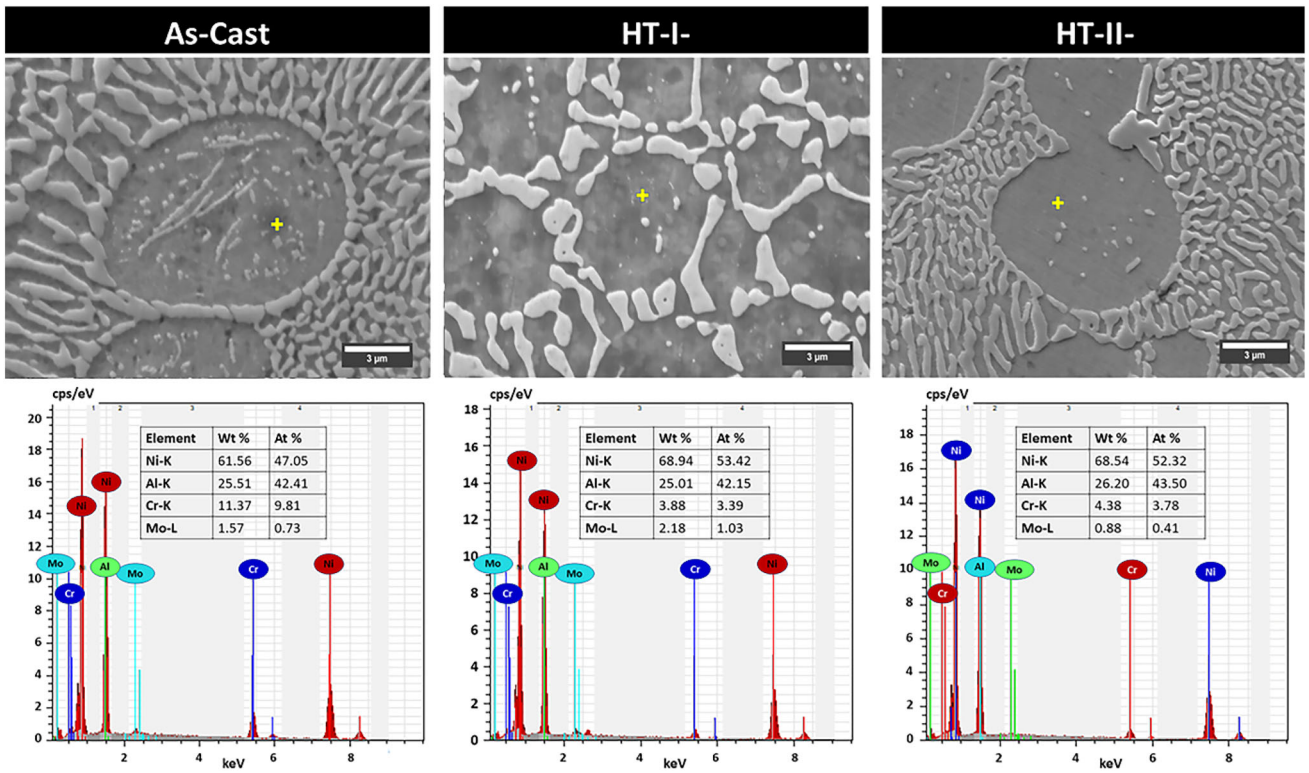

Figure 2. EDS point analysis of NiAl-based (dark) phase in as-cast and heat-treated NiAl–Cr(Mo) alloys.

The minor amount of Nd addition considerably alters the microstructure of the alloy: (i) NiAl/Cr(Mo) eutectic lamella is refined strongly. The interlamellar spacing within the eutectic cell is decreased compared to that of without Nd addition. The interlamellar spacing of the eutectic for Nd-free and Nd-containing alloys are calculated as 0.65 ± 0.014 µm and 0.45 ± 0.009 µm, respectively. (ii) the NiAl and Cr(Mo) phases close to the eutectic cell boundary become coarser, (iii) the size of the eutectic cells are decreased markedly, and (iv) small Nd-rich phases start to form within the eutectic cells.

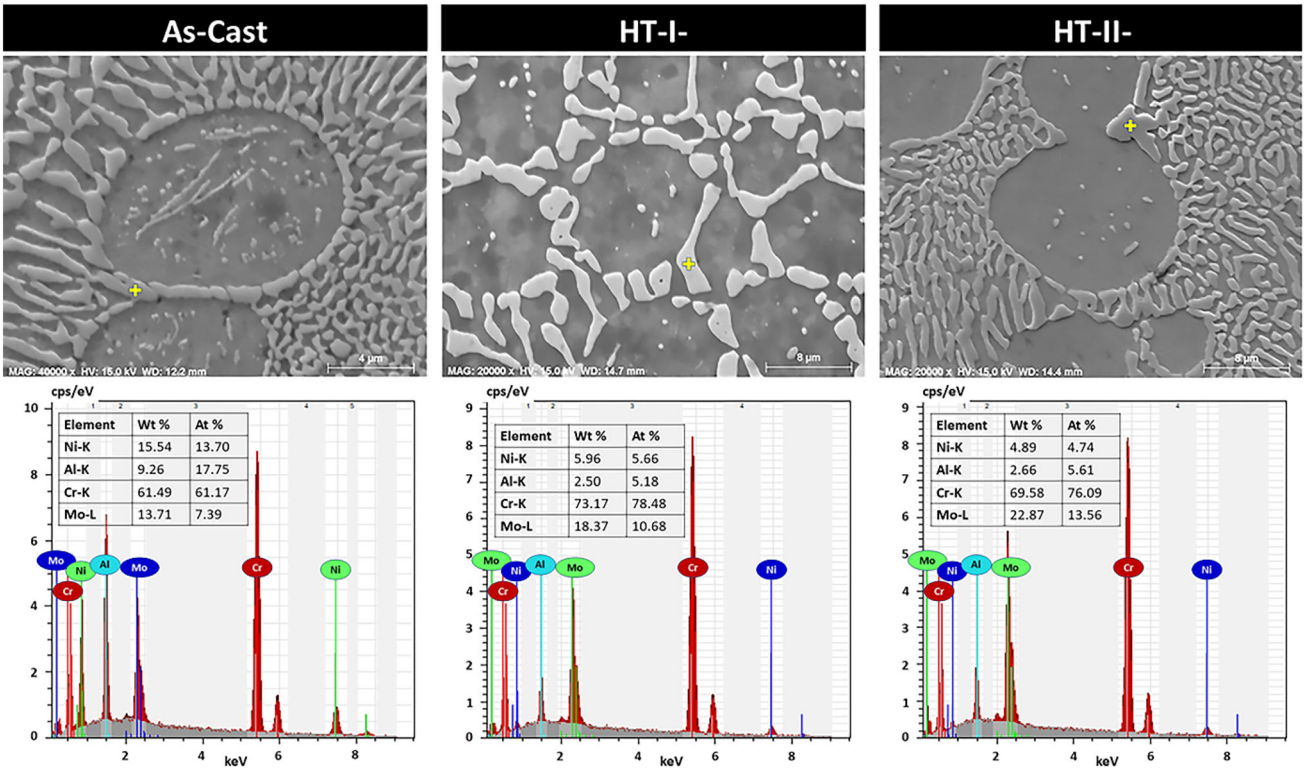

Figure 3. EDS point analysis of Cr(Mo) based (light) phase in as-cast and heat-treated NiAl–Cr(Mo) alloys.

The results of the EDS analysis (Figures 4, 5) reveal that Nd is uniformly distributed in the NiAl and Cr(Mo) phases. Cr(Mo) phase dissolves a slightly higher amount of Nd compared to the NiAl phase. Additionally, the EDS mapping analysis shows that Nd is uniformly distributed along the eutectic cell boundaries and cell interior. No Nd-rich regions or phases are observed in the microstructure of NiAl–Cr(Mo)–Nd alloys.

After the first heat treatment of 1250 °C/48 h furnace cooling (HT-I) Cr(Mo) lamellas coarsen significantly in the microstructures of both Nd-free and a minor amount of Nd-containing alloys. The lamellas spheroidize and transform to particles. Although the coarsening also occurs after the second heat-treatment of 1250 °C/48 h quenching and subsequent aging (HT-II), the amount of coarsening is noticeably less compared to HT-I. A typical microstructure that is composed of alternating lamella or fibers of two different phases can be produced after eutectic phase transformation. In this microstructure, the minor phase is embedded in the continuous matrix phase.[24,25] At high temperatures, fine eutectic lamella microstructures can coarsen in order to reach thermodynamic equilibrium. In the basic theory of the coarsening, phases tend to reduce the total energy by decreasing the surface energy via minimizing the interfacial area of the relevant phases.[10,23,24] In the present study, the coarsening of eutectic after HT-I is relatively higher than that of HT-II. Compared to HT-II, relatively higher coarsening in HT-I accelerates the diffusion kinetics and coarsens the lamellas much more.

The effect of coarsening is clearly observed in microhardness measurements (Table 2). For both compositions, the as-cast alloys exhibit the highest mean microhardness value. After heat-treatment, the mean microhardness values are decreased as a result of coarsening. The samples heat-treated at 1250 °C/48 h furnace cooling (HT-I) exhibit the lowest microhardness values since they possess the coarsest microstructure. Moreover, a minor amount of Nd addition increases the mean microhardness values of NiAl–Cr(Mo) alloys because of the refinement effect of Nd. Normally, it is expected that increase in mean microhardness value would result in a decrease in ductility or toughness which further increase the brittle nature of NiAl based alloys. However, NiAl–Cr(Mo) based alloys with rare-earth element additions can exhibit best combination of mechanical properties: enhanced ductility with increased strength/hardness. Guo et al.[26] presented that 0.005, 0.05 or 0.1 wt% rare-earth element (Y, Ce, Nd and Dy) containing NiAl–Cr(Mo, Hf) based eutectic alloys showed higher strength and strain values compared to those for rare-earth free alloy. However, for higher rare-earth addition (0.5 wt%) the alloy became brittle. Similarly, Guo et al.[5] also showed that both strength and ductility of NiAl–Cr(Mo)–Ho alloy increase with increasing Ho content up to 0.1 at%. Further increasing Ho content decreased the strength and ductility. Therefore, based on the present results, it is expected that 0.1 at% Nd addition would increase the strength/hardness and ductility of NiAl–Cr(Mo) eutectic alloy.

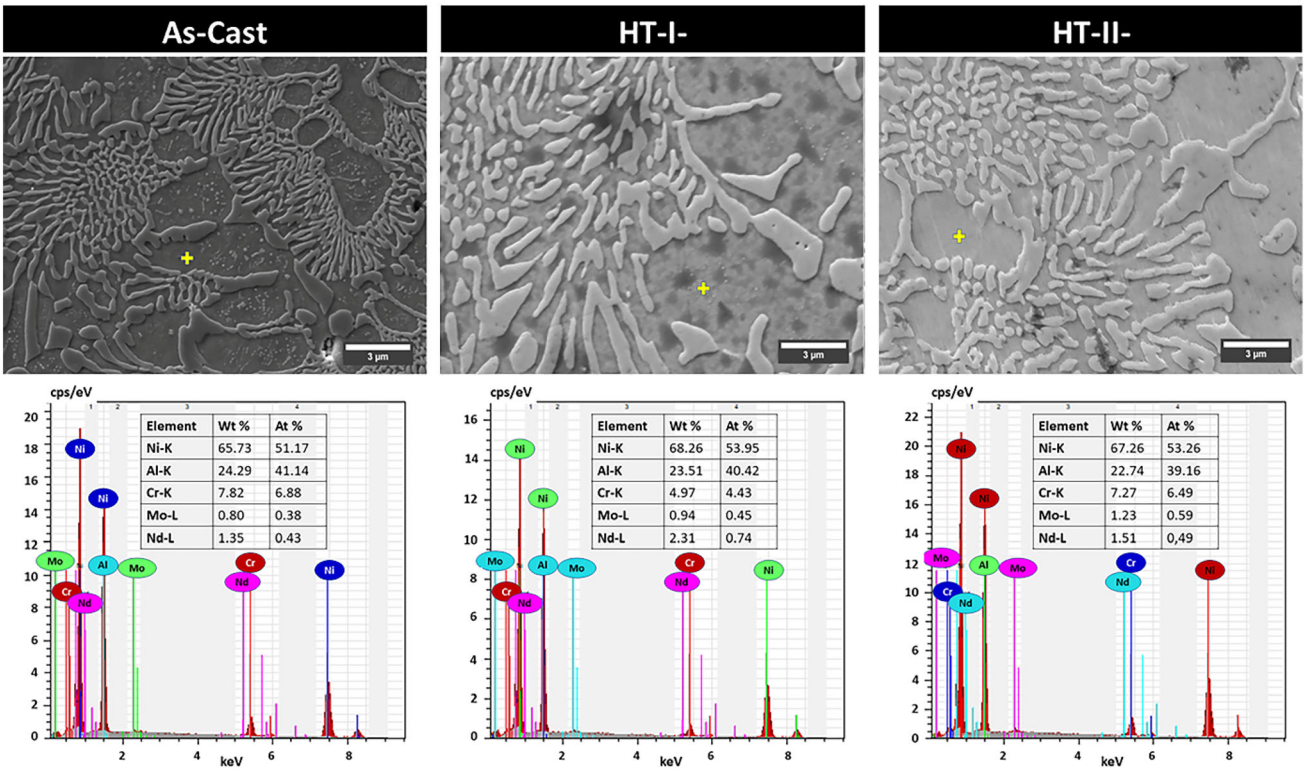

Figure 4. EDS point analysis of NiAl-based (dark) phase in as-cast and heat-treated NiAl–Cr(Mo)–Nd alloys.

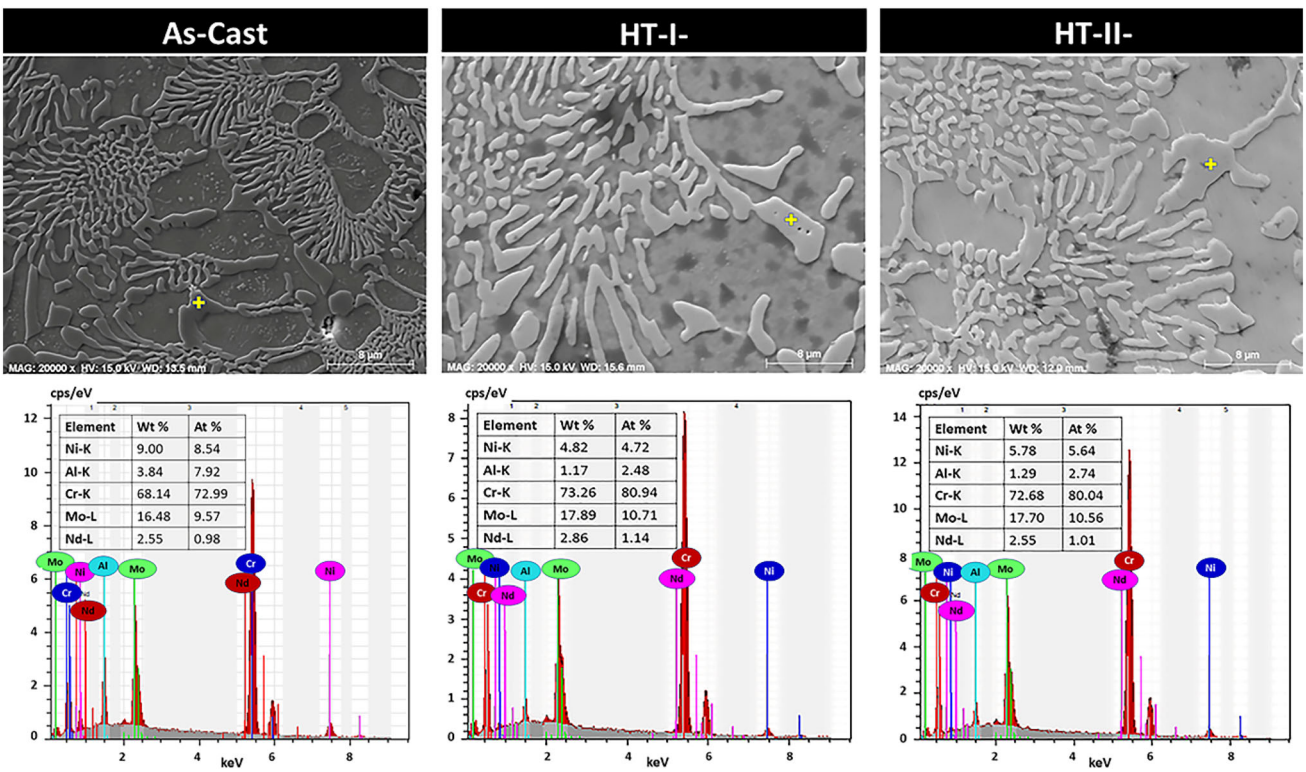

Figure 5. EDS point analysis of Cr(Mo) based (light) phase in as-cast and heat-treated NiAl–Cr(Mo)–Nd alloys.

The phase analysis of the NiAl–Cr(Mo) and NiAl–Cr(Mo)–Nd alloys are investigated by XRD analysis, as shown in Figure 6. It is obvious that both alloys are composed of NiAl matrix (JCPDS Card No: 44-1188) and Cr(Mo) (JCPDS Card No: 06-0694) phases. The (110) crystal planes are the strongest diffraction peaks of the NiAl and

Table 2. Mean Microhardness Values of As-Cast and Heat-Treated NiAl–Cr(Mo) and NiAl–Cr(Mo)–Nd Alloys

Condition	Microhardness (HV)	
	NiAl–Cr(Mo)	NiAl–Cr(Mo)–Nd
As-cast	497 ± 4	532 ± 2
HT-I-	438 ± 5	448 ± 4
HT-II-	449 ± 4	495 ± 4

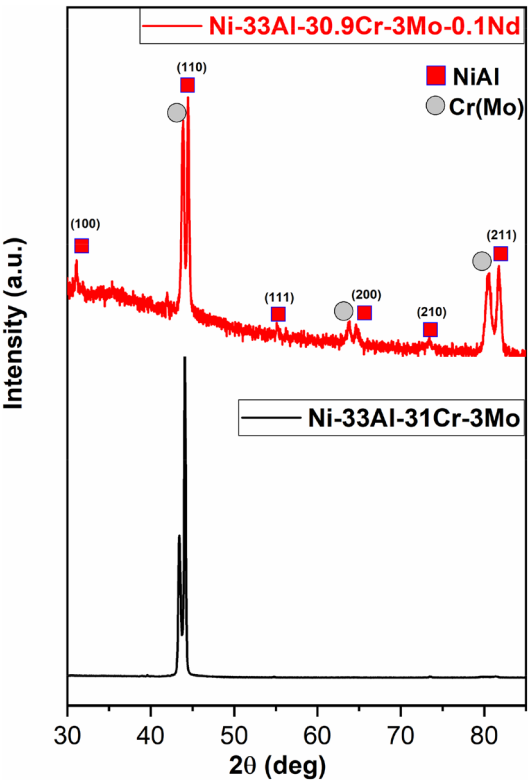

Figure 6. XRD diffraction patterns of as-cast NiAl–Cr(Mo) and NiAl–Cr(Mo)–Nd alloys.

Cr(Mo) phases. Moreover, the XRD pattern of NiAl–Cr(Mo)–Nd alloy reveals that the intensity of the diffraction peak corresponding to the (211) plane is higher for the NiAl phase than Cr(Mo) phase. This result indicates that the addition of Nd may impede the growth of Cr(Mo) during the solidification process. A similar finding is also observed in the previous research[11,12,27] regarding the Hf and Ho addition to the NiAl–Cr(Mo) eutectic alloys. In addition, the formation of any other phase is not observed in the XRD analysis.

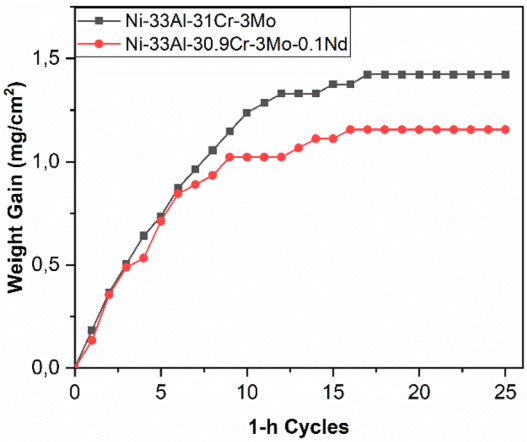

Figure 7. Mass gain vs. time plot for as-cast samples at 1000 °C.

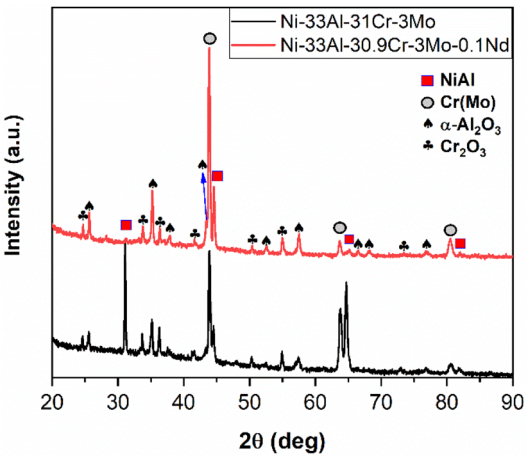

Figure 8. XRD patterns of the surfaces of as-cast NiAl–Cr(Mo) and NiAl–Cr(Mo)–Nd samples after cyclic oxidation at 1000 °C.

Cyclic Oxidation Test

The weight gain per unit area of the studied alloys as a function of oxidation time is given in Figure 7. The plots of both alloys show two distinct oxidation periods: the first period with rapid oxidation (0–12 h) and the final period with slower oxidation (13–25 h). The slopes of the first period are clearly sharper than in comparison with the slopes of the second period. A certain amount of scale spallation is observed during the cyclic oxidation tests. Comparing the weight change plots of two alloys, the weight gain of the NiAl–Cr(Mo) alloy is more pronounced.

Table 3. Parabolic Rate Constants for As-Cast Samples

Alloy	k_p^I (mg^2 cm^{-4} sn^{-1})	k_p^{II} (mg^2 cm^{-4} sn^{-1})
NiAl–Cr(Mo)	$4.47 \times 10^{-5} \pm 1.54 \times 10^{-6}$	$6.03\text{x}10^{-6} \pm 1.11 \times 10^{-6}$
NiAl–Cr(Mo)–Nd	$3.42 \times 10^{-5} \pm 1.89 \times 10^{-6}$	$6.02\text{x}10^{-6} \pm 8.81 \times 10^{-7}$

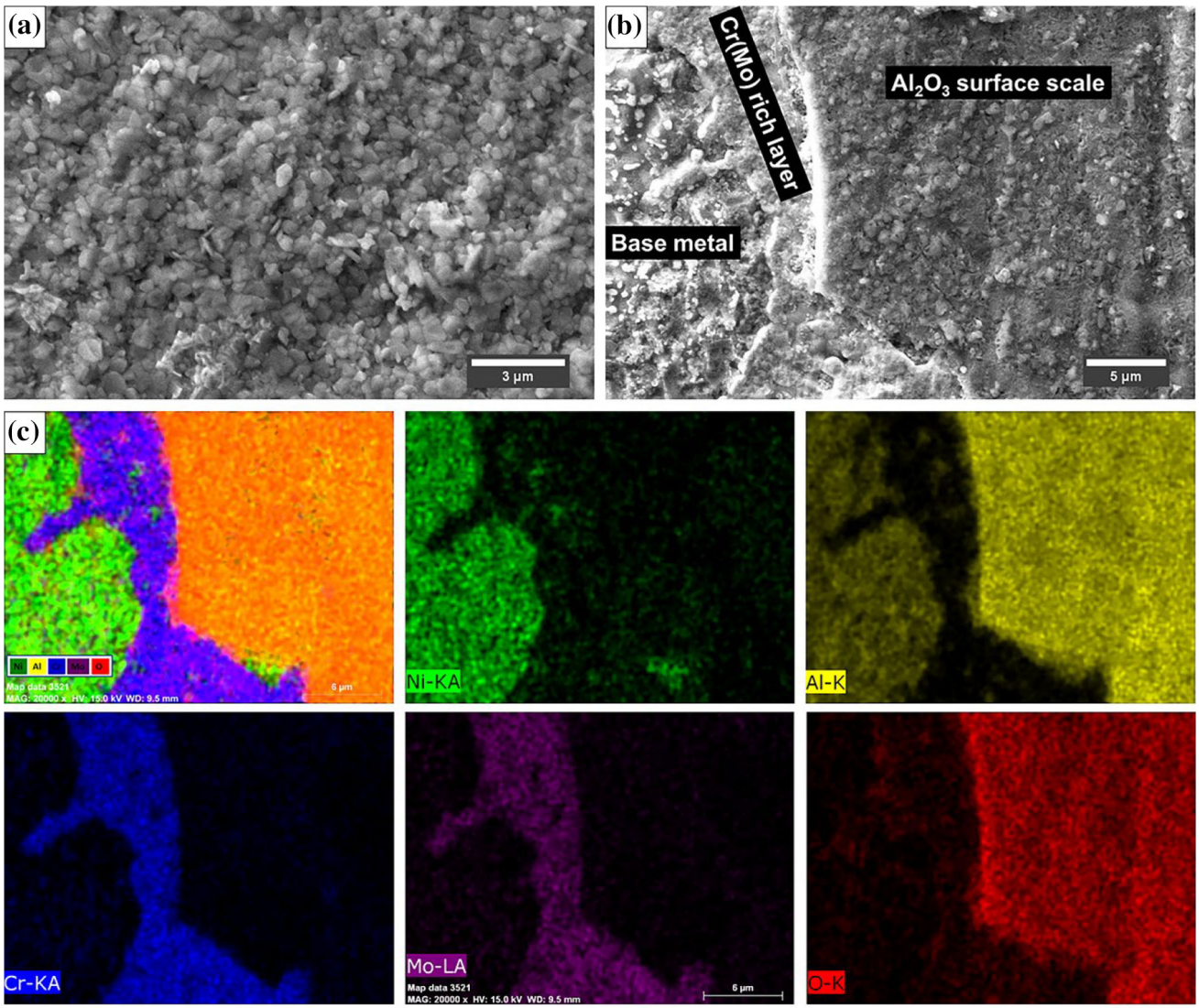

Figure 9. Surface scale morphology and EDS elemental mapping of NiAl–Cr(Mo) samples oxidized at 1000 °C; (a) surface scale showing the spalled region, (b) Al_2O_3 scale, and (c) EDS elemental mapping.

In order to examine the oxidation kinetics, the weight gain plots can be fitted to a power law equation[7];

$$\left(\Delta W/A\right)^n = kt \qquad \text{Eqn. 1}$$

where t is the exposure time, k is the oxidation rate constant, A is the surface area of the sample, ΔW is the weight gain and n is the power law exponent. The inverse value of power law exponents can be calculated from the slope of a linear regression line of the double logarithm (ΔW/A) vs t curves. If the value of n is equal to 2, the oxidation kinetics obey a parabolic rate law. The fitting quality standard (R, correlation coefficient) is at least 0.99746.

According to the calculated exponents, only NiAl–Cr(Mo) alloy obeys parabolic kinetics in the initial oxidation period. The calculated power law exponents for NiAl–Cr(Mo)–Nd and NiAl–Cr(Mo) alloy in the second period are different from 2. Therefore, a parabolic behavior may not occur and a parabolic rate constant (k_p) may not be calculated correctly. In several studies regarding the oxidation kinetics of similar alloys,[28–31] the apparent parabolic rate constant can be calculated from the parabolic rate law ($n = 2$). The calculated $k_{p,\ app}$ values for both alloys and two oxidation periods are listed in Table 3.

Compared to the NiAl–Cr(Mo) alloy, the NiAl–Cr(Mo)–Nd alloy has somewhat lower $k_{p,app}$ values which implies a decrease in oxidation rate after Nd addition. For the first period, the k_p values of both alloys are in the same order of magnitude (10^{-5} mg^2 cm^{-4} sn^{-1}), which agrees well with the k_p values of similar compositions in the literature.[32–35] For longer oxidation times (>12 h), a considerably lower oxidation rate is observed for both alloys. The $k_{p,app}$ values of both alloys are similar in the second period.

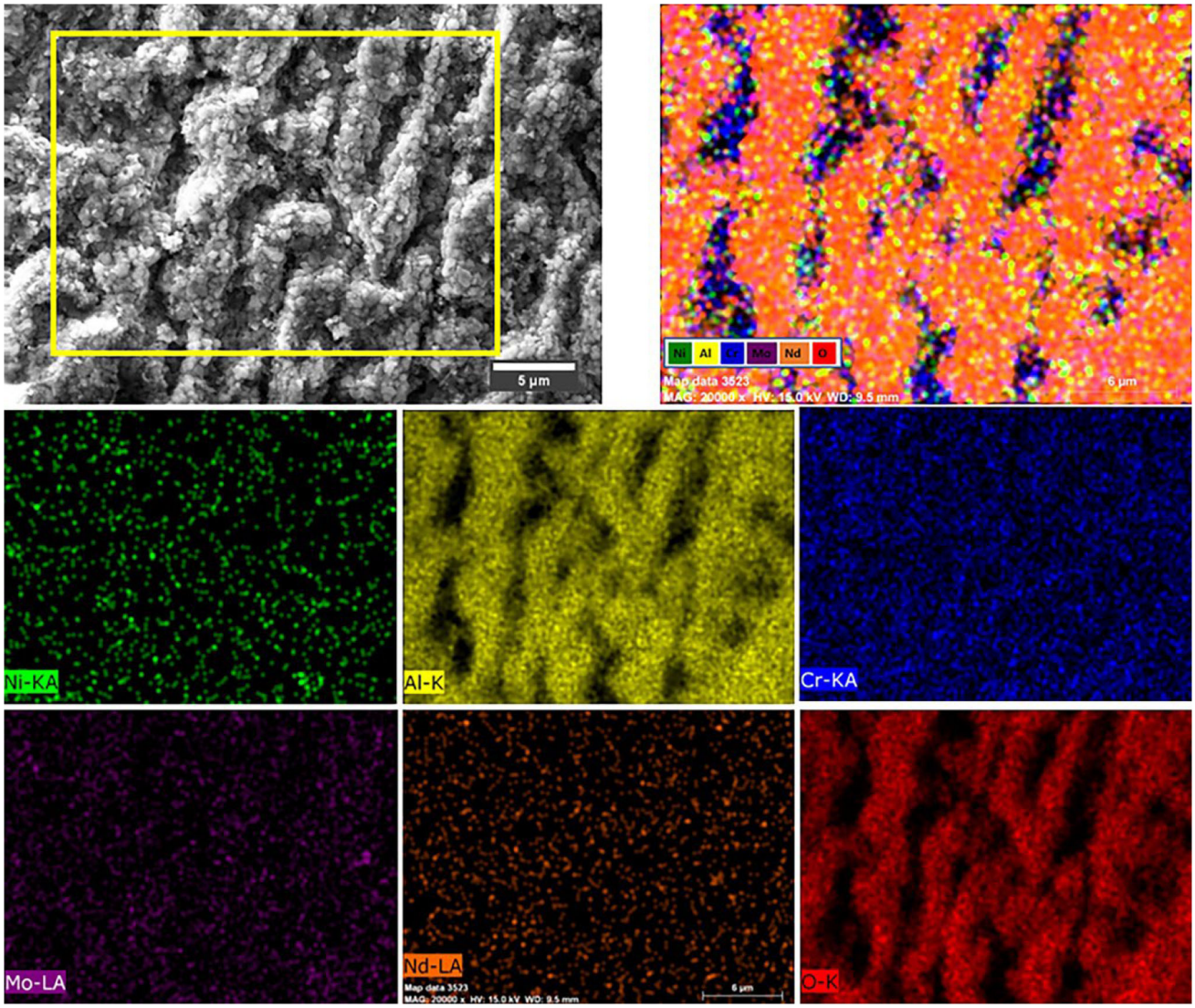

Figure 10. Surface scale morphology and EDS elemental mapping of NiAl–Cr(Mo)–Nd samples oxidized at 1000 °C.

The XRD patterns of both alloys after cyclic oxidation tests are shown in Figure 8. The scale is composed of α-Al_2O_3 (JCPDS Card No: 042-1468) and Cr_2O_3 (JCPDS Card No: 38-1479). Besides α-Al_2O_3 and Cr_2O_3, any other oxides, i.e., θ-Al_2O_3, NiO, $NiAl_2O_4$, and $NiMo_4$, are not detected. The presence of substrate peaks indicates the thin oxide scale thickness and scale spallation.

Figure 9 shows the surface scale morphology of the NiAl–Cr(Mo) alloy after cyclic oxidation at 1000 °C. The surface scale is composed of α-Al_2O_3 as shown in Figure 9a. After cyclic oxidation, scale spallation (Figure 9b) and cracks are observed. The spallation occurs due to the thermal stresses originating through from the heating/cooling cycles. In addition, elemental mapping analyses (Figure 9c) show that a Cr(Mo)-rich layer is present between the surface scale and metallic substrate.

The surface scale of the Nd-added specimen is shown in Figure 10. The surface scale is composed of fine and equiaxed α-Al_2O_3 grains. Moreover, no important scale spallation and cracks are observed. However, investigation of the surface scale morphologies does not indicate the entire oxidation process. Internal oxidation can occur under the surface scale.[17,36] Therefore, cross-sectional SEM-EDS analyses (Figure 11) are conducted. The results indicate that the oxide scale of NiAl–Cr(Mo) alloy consists of an α-Al_2O_3 surface layer (Figure 11a) with little Cr_2O_3 nodules (Figure 12) and a Cr(Mo)-rich layer is formed in the metal/oxide interface. The formation of Cr_2O_3 particles is confirmed with EDS point analysis in the cross-sectional examination. For the Nd-added alloy, the cross-sectional analyses (Figure 11b) reveal that the surface layer is mainly composed of α-Al_2O_3 and little Cr_2O_3 protective scale. Similar to base alloy, a Cr(Mo)-rich layer is also formed in the metal/oxide interface.

For NiAl-Cr(Mo) alloy, the continuous heating-cooling cycles occurring in the surface region generate internal stresses which lead to scale spallation. A substantial Al

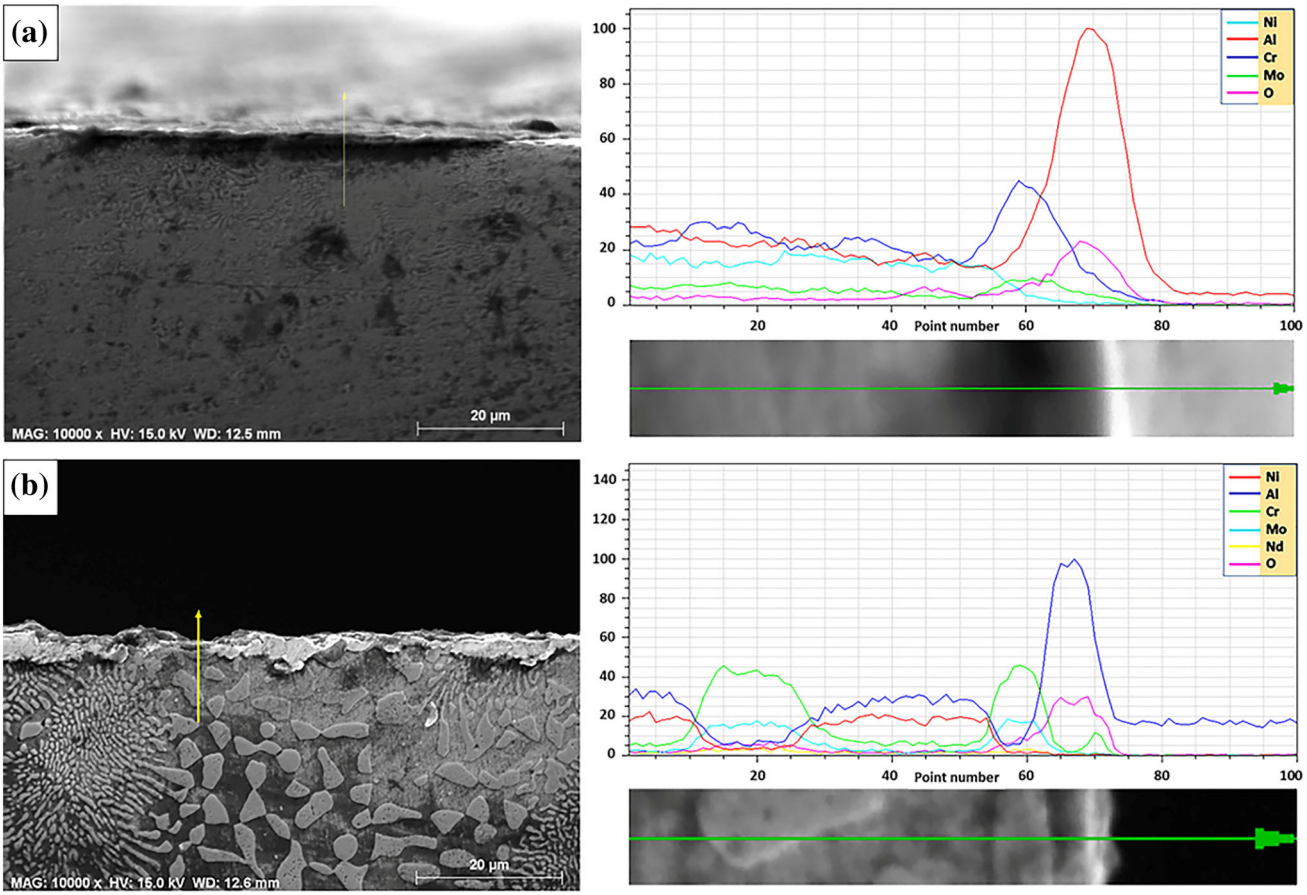

Figure 11. Cross-sectional SEM-EDS surface oxide analysis of (a) NiAl–Cr(Mo) and (b) NiAl–Cr(Mo)–Nd alloys oxidized at 1000 °C.

depletion occurs due to continuous scale spallation and formation of the Al_2O_3 scale. Thus, the elimination of Al leads to the formation of the Cr(Mo) layer on the alloy surface.[7,37] On the other hand, the trace amount of Nd addition results in important improvements in the oxidation resistance of NiAl-Cr(Mo) alloy. With Nd addition, the oxidation mass gain is decreased, scale spallation is extensively reduced and the adhesion of the oxide scale is promoted. It is believed that a trace amount of rare earth Nd addition promotes the inward diffusion of O which results in the removal of interspaces in the oxide scale. Thus, a reduction of mass gain is observed. Moreover, the refinement of microstructure as a result of Nd addition may support the Al_2O_3 layer to wrap the Cr(Mo) phase quickly. Therefore, the Cr(Mo) layer may be formed more easily between the surface scale and metallic substrate, which has the possibility to reduce the internal stresses and enhance the scale adhesion.[37]

The higher concentration of Al in the NiAl matrix phase could promote the development of an Al_2O_3 scale in the oxidation process. At the same time, the Cr(Mo) phase is also exposed to air and oxidation occurs. The Mo oxides (i.e., MoO_3) are volatile and non-protective, which accelerates the oxidation process and contributes to the reduction of the oxidation mass gain at high temperatures.[7,38–40] However, a protective Cr_2O_3 scale and volatile CrO_3 can be formed as a result of the oxidation of Cr. Protective Cr_2O_3 forms at relatively lower testing temperatures ($T \leq 1000$ °C), while non-protective CrO_3 forms at higher temperatures.[41–44] In the present study, we observe the formation of protective Cr_2O_3 nodules based on the results of the XRD and EDS analysis.

Furthermore, the absence of NiO on the scale seems to be an advantage of the studied compositions. Unlike Cr_2O_3 and Al_2O_3, NiO is a non-protective oxide and does not protect metallic substrate against oxidation. The formation of NiO is strongly depends on the alloy composition, especially Ni concentration. NiO is easily formed on the outers urfaces of Ni-rich alloys containing higher than 70 at% Ni.[45] In the present study, the NiO formation is not observed since the Ni concentration of the studied alloys are considerably lower than 70 at%.

The addition of reactive elements such as Y, Ce, Zr, and Hf to NiAl-based alloys is considered to be beneficial for oxide scale adhesion and have also several positive effects on the microstructure and mechanical properties of NiAl-based alloys.[46–50] However, like other rare-earth elements

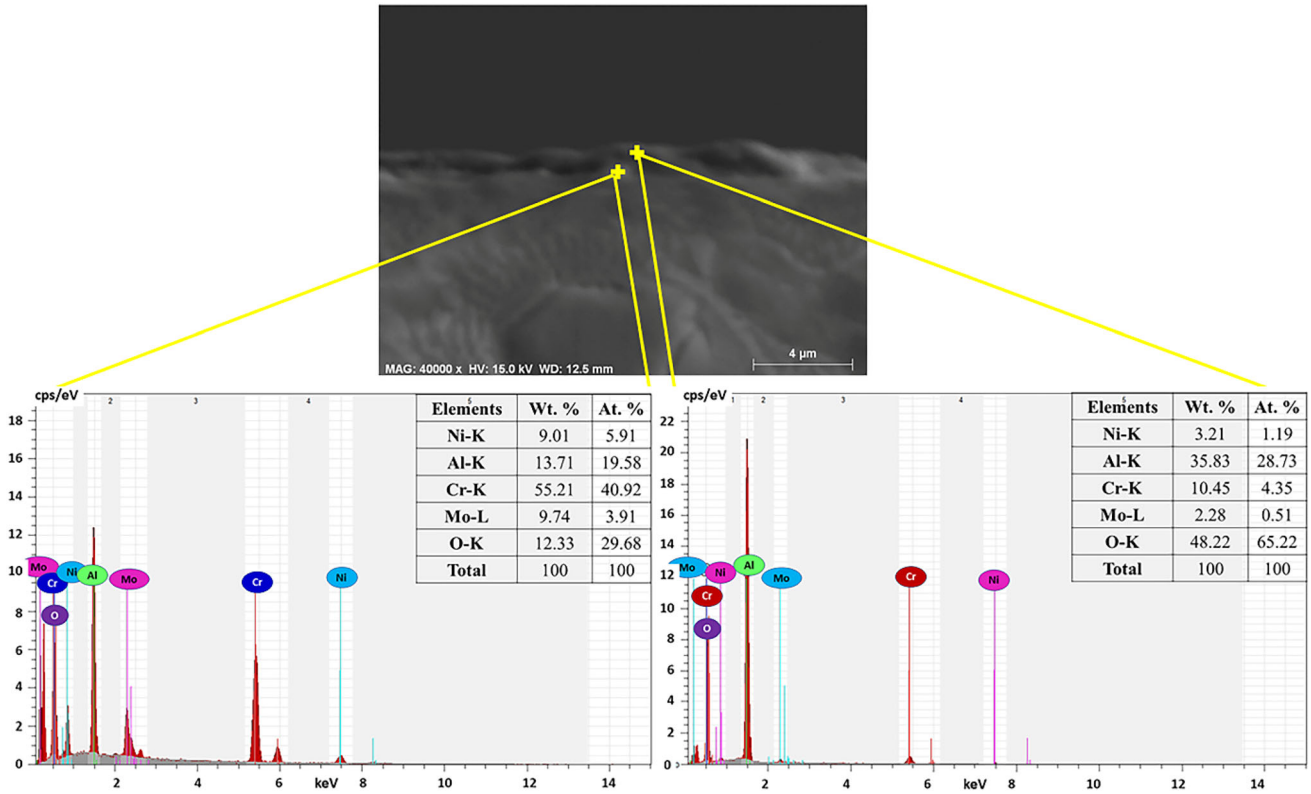

Figure 12. EDS point analysis of Cr_2O_3 nodule and Al_2O_3 surface scale in NiAl–Cr(Mo) alloy oxidized at 1000 °C.

Dy and Ho, Nd has higher chemical reactivity compared to reactive elements Y, Ce, Hf, and Zr.[7,37] In the oxidation process, Nd addition influences both surface oxide and metallic substrate. For rare-earth element additions, microstructural refinement takes place because of the formation of non-spontaneous cores and the reactivity of the surfaces. Therefore, Al_2O_3 covers the surface and a Cr(Mo)-rich layer forms at the metal/oxide interface.[7]

Conclusions

The effect of trace amount of Nd addition on the microstructure, microhardness, and cyclic oxidation behavior of Ni–33Al–31Cr–3Mo alloy is studied in detail, and the main conclusions can be stated as follows:

i. The microstructures of both compositions are composed of NiAl and Cr(Mo) phases.
ii. Addition of 0.1 at% Nd into Ni–33Al–31Cr–3Mo alloy refines the eutectic microstructure within the eutectic cells and increases the mean microhardness value.
iii. Protective α-Al_2O_3 and Cr_2O_3 scales form on the surfaces of both alloys.
iv. A Cr(Mo) rich phase is observed on the metal/oxide interface of both alloys.
v. With Nd addition, oxidation resistance is considerably improved with better scale adhesion and reduced mass gain.

Authors' Contribution

MSA: Conceptualization, Methodology, Writing—original draft. MY: Investigation, Methodology, Writing—review & editing.

Funding

No funding was received to assist with the preparation of this paper.

Conflict of interest The authors declare that they have no known competing financial interests or personal relationships that could have appeared to influence the work reported in this paper.

REFERENCES

1. K.S. Chan, The fracture toughness of niobium-based, in situ composites. Metall. and Mater. Trans. A. **27**, 2518–2531 (1996)
2. A. Misra, R. Gibala, Plasticity in multiphase intermetallics. Intermetallics **8**, 1025–1034 (2000)
3. R.D. Noebe, R.R. Bowman, M.V. Nathal, Physical and mechanical properties of the B_2 compound NiAl. Int. Mater. Rev. **38**, 193–232 (1993)

4. Z. Shang, Q. Zhang, J. Shen, H. Bai, X. Dong, W. Bai, L. Zhong, G. Liu, Y. Xu, Effects of Nb/Ti additions and heat treatment on the microstructure evolution and hardness of as-cast and directionally solidified NiAl–Cr (Mo) alloy. J. Market. Res. **10**, 905–915 (2021)
5. J. Guo, L. Sheng, Y. Tian, L. Zhou, H. Ye, Effect of Ho on the microstructure and compressive properties of NiAl-based eutectic alloy. Mater. Lett. **62**, 3910–3912 (2008)
6. L. Wang, J. Shen, Z. Shang, J. Zhang, J. Chen, H. Fu, Effect of Dy on the microstructures of directionally solidified NiAl–Cr (Mo) hypereutectic alloy at different withdrawal rates. Intermetallics **44**, 44–54 (2014)
7. G. Zhang, H. Zhang, J. Guo, Improvement of cyclic oxidation resistance of a NiAl-based alloy modified by Dy. Surf. Coat. Technol. **201**, 2270–2275 (2006)
8. D. Miracle, Overview No. 104 the physical and mechanical properties of NiAl. Acta Metall. et Mater. **41**, 649–684 (1993)
9. L. Wang, J. Shen, Effect of heat treatment on the microstructure and elevated temperature tensile property of Fe-doped NiAl–Cr (Mo)–(Hf, Dy) eutectic alloy. Mater. Sci. Eng. A **654**, 177–183 (2016)
10. H. Li, J. Guo, K. Huai, H. Ye, Microstructure characterization and room temperature deformation of a rapidly solidified NiAl-based eutectic alloy containing trace Dy. J. Cryst. Growth **290**, 258–265 (2006)
11. L.-Y. Sheng, Y. Fang, T.-F. Xi, Y.-F. Zheng, J.-T. Guo, Microstructure and room temperature mechanical properties of NiAl–Cr (Mo)–(Hf, Dy) hypoeutectic alloy prepared by injection casting. Trans. Nonferrous Metals Soc. China **23**, 983–990 (2013)
12. L. Zheng, L. Sheng, Y. Qiao, Y. Yang, C. Lai, Influence of Ho and Hf on the microstructure and mechanical properties of NiAl and NiAl-Cr (Mo) eutectic alloy. Mater. Res. Expr. **6**, 046502 (2019)
13. J. Peng, X. Fang, Z. Qu, J. Wang, Isothermal oxidation behavior of NiAl and NiAl-(Cr, Mo) eutectic alloys. Corros. Sci. **151**, 27–34 (2019)
14. H. Grabke, Oxidation of NiAl and FeAl. Intermetallics **7**, 1153–1158 (1999)
15. E. George, C. Liu, Brittle fracture and grain boundary chemistry of microalloyed NiAl. J. Mater. Res. **5**, 754–762 (1990)
16. H.J. Grabke, M.W. Brumm, B. Wagemann, The oxidation of NiAl. Mater. Corros.—Werkst. und Korros. **47**, 675–677 (1996). https://doi.org/10.1002/maco.19960471203
17. M. Yildirim, M.S. Atas, M.V. Akdeniz, A.O. Mekhrabov, Effect of Y addition on the structural properties and oxidation behavior of Fe60Al40-nYn Alloys (n = 1, 3, and 5 at%). Mater. High Temp. **39**, 220–230 (2022)
18. M.S. Atas, M. Yildirim, Morphological development, coarsening, and oxidation behavior of Ni-Al-Nb superalloys. J. Mater. Eng. Perform. **29**, 4421–4434 (2020)
19. M.S. Atas, M. Yildirim, Temporal evolution, coarsening behavior and oxidation resistance of Ni–15Al superalloy. J. Alloy. Compd. **809**, 151784 (2019)
20. A. Demirel, E.C. Cetin, A. Karakus, M.S. Atas, M. Yildirim, Microstructural evolutions and oxidation behavior of Fe-4Cr-6Ti ferritic alloy with Fe2Ti laves phase precipitates. Arch. Metall. Mater. **67**, 827–836 (2022). https://doi.org/10.24425/amm.2022.139672
21. M.S. Atas, M. Yildirim, Structural properties and cyclic oxidation behavior of NiAlY superalloys. Kov. Mater.—Metall. Mater. **60**, 281–292 (2022). https://doi.org/10.31577/km.2022.5.281
22. L. Sheng, L. Wang, T. Xi, Y. Zheng, H. Ye, Microstructure, precipitates and compressive properties of various holmium doped NiAl/Cr (Mo, Hf) eutectic alloys. Mater. Des. **32**, 4810–4817 (2011)
23. M. Yildirim, M.V. Akdeniz, A.O. Mekhrabov, Microstructural evolution and room-temperature mechanical properties of as-cast and heat-treated Fe50Al50−nNbn alloys (n = 1, 3, 5, 7, and 9 at%). Mater. Sci. Eng., A **664**, 17–25 (2016)
24. X. Li, F. Bottler, R. Spatschek, A. Schmitt, M. Heilmaier, F. Stein, Coarsening kinetics of lamellar microstructures: experiments and simulations on a fully-lamellar Fe–Al in situ composite. Acta Mater. **127**, 230–243 (2017)
25. A.J. Ardell, Coarsening of directionally-solidified eutectic microstructures, Computer-aided Design of High-temperature Materials, 163-182 (1999).
26. J. Guo, K. Huai, Q. Gao, W. Ren, G. Li, Effects of rare earth elements on the microstructure and mechanical properties of NiAl-based eutectic alloy. Intermetallics **15**, 727–733 (2007)
27. L. Sheng, J. Guo, W. Ren, Z. Zhang, Z. Ren, H. Ye, Preliminary investigation on strong magnetic field treated NiAl–Cr (Mo)–Hf near eutectic alloy. Intermetallics **19**, 143–148 (2011)
28. D. Zander, R.D. Pütz, Investigation of the microstructure related high temperature oxidation behaviour of Fe–25Al–5Cr-0.5 Zr and Fe–25Al–5Cr-0.5 Zr+ TiC at 700° C in air. Intermetallics **126**, 106924 (2020)
29. K. Nowak, M. Kupka, High-temperature oxidation behaviour of B_2 FeAl based alloy with Cr Zr and B additions. Mater. Chem. Phys. **132**, 902–908 (2012). https://doi.org/10.1016/j.matchemphys.2011.12.031
30. L. Senčekova, M. Palm, J. Pešička, J. Veselý, Microstructures, mechanical properties and oxidation behaviour of single-phase Fe_3Al (D03) and two-phase α-Fe, Al (A_2)+Fe_3Al (D03) FeAlV alloys. Intermetallics **73**, 58–66 (2016). https://doi.org/10.1016/j.intermet.2016.03.004
31. A. Hotař, M. Palm, Oxidation resistance of Fe–25Al–2Ta (at%) in air. Intermetallics **18**, 1390–1395 (2010). https://doi.org/10.1016/j.intermet.2010.02.014

32. H. Guo, D. Li, L. Zheng, S. Gong, H. Xu, Effect of co-doping of two reactive elements on alumina scale growth of β-NiAl at 1200°C. Corros. Sci. **88**, 197–208 (2014). https://doi.org/10.1016/j.corsci.2014.07.036
33. Y. Garip, C. Ceper, N. Ergin, A.S. Demirkıran, O. Ozdemir, Production of NiAl–(Cr, Mo) eutectic alloys and their cyclic oxidation behavior at 800–1000°C. Phys. Metals Metall. **121**, 1301–1308 (2020). https://doi.org/10.1134/S0031918X20130062
34. B. Han, Y. Ma, H. Peng, L. Zheng, H. Guo, Effect of Mo, Ta, and Re on high-temperature oxidation behavior of minor Hf doped β-NiAl alloy. Corros. Sci. **102**, 222–232 (2016). https://doi.org/10.1016/j.corsci.2015.10.011
35. P. Castello, F.H. Stott, F. Gesmundo, Yttrium-promoted selective oxidation of aluminium in the oxidation at 1100°C of an eutectic Ni–Al–Cr_3C_2 alloy. Corros. Sci. **41**, 901–918 (1999). https://doi.org/10.1016/S0010-938X(98)00162-0
36. M.S. Atas, M. Yildirim, Structural properties and cyclic oxidation behavior of Ni–Al–Y superalloys. Kovove Mater. **60**, 281–292 (2022)
37. Z.-S. Wang, X. Yi, J.-T. Guo, L.-Z. Zhou, Z.-Q. Hu, G.-Y. Zhang, Z.-G. Chen, High temperature oxidation behavior of directionally solidified NiAl–31Cr–2.9 Mo–0.1 Hf–0.05 Ho eutectic alloy. Trans. Nonferrous Metals Soc. China **22**, 1582–1587 (2012)
38. A. Martinez-Villafane, J. Chacon-Nava, C. Gaona-Tiburcio, F. Almeraya-Calderon, R. Bautista-Margulis, J. Gonzalez-Rodríguez, The effect of Nd and Pr on the oxidation behavior of a Fe-13Cr alloy. Scripta Mater. **46**, 127–130 (2002)
39. J. Guo, C. Xu, Effect of NiAl microcrystalline coating on the high-temperature oxidation behavior of NiAl–28Cr–5Mo–1Hf. Oxid. Met. **58**, 457–468 (2002)
40. J.L. González-Carrasco, P. Perez, P. Adeva, J. Chao, Oxidation behaviour of an ODS NiAl-based intermetallic alloy. Intermetallics **7**, 69–78 (1999)
41. Q. Feng, B. Tryon, L.J. Carroll, T.M. Pollock, Cyclic oxidation of Ru-containing single crystal superalloys at 1100°C. Mater. Sci. Eng., A **458**, 184–194 (2007). https://doi.org/10.1016/j.msea.2006.12.064
42. J. Huang, H. Fang, X. Fu, F. Huang, H. Wan, Q. Zhang, S. Deng, J. Zu, High-temperature oxidation behavior and mechanism of a new type of wrought Ni–Fe–Cr–Al superalloy up to 1300°C. Oxidat. Metals **53**, 273–287 (2000). https://doi.org/10.1023/A:1004537119922
43. P. Berthod, Kinetics of high temperature oxidation and chromia volatilization for a binary Ni–Cr alloy. Oxidat. Metals **64**, 235–252 (2005). https://doi.org/10.1007/s11085-005-6562-8
44. M.H. Li, X.F. Sun, J.G. Li, Z.Y. Zhang, T. Jin, H.R. Guan, Z.Q. Hu, Oxidation behavior of a single-crystal Ni-base superalloy in air. I: at 800 and 900°C. Oxidat. Metals **59**, 591–605 (2003). https://doi.org/10.1023/A:1023604214245
45. G. Wallwork, A. Hed, Some limiting factors in the use of alloys at high temperatures. Oxid. Met. **3**, 171–184 (1971)
46. T. Boll, K.A. Unocic, B.A. Pint, A. Mårtensson, K. Stiller, Grain boundary chemistry and transport through alumina scales on NiAl alloys. Oxid. Met. **88**, 469–479 (2017)
47. T. Boll, K.A. Unocic, B.A. Pint, K. Stiller, Interfaces in oxides formed on NiAlCr doped with Y Hf, Ti, and B. Microsc. Microanal. **23**, 396–403 (2017)
48. J.A. Haynes, B.A. Pint, Y. Zhang, I.G. Wright, Comparison of the cyclic oxidation behavior of β-NiAl, β-NiPtAl and γ–γ′ NiPtAl coatings on various superalloys. Surf. Coat. Technol. **202**, 730–734 (2007)
49. B. Pint, K. More, I. Wright, Effect of quaternary additions on the oxidation behavior of Hf-doped NiAl. Oxid. Met. **59**, 257–283 (2003)
50. B. Pint, M. Treska, L. Hobbs, The effect of various oxide dispersions on the phase composition and morphology of Al_2O_3 scales grown on β-NiAl. Oxid. Met. **47**, 1–20 (1997)